

Heralded generation of a three-mode NOON state

Sukhjit P. Singh,¹ Elnaz Bazzazi,² Diego N. Bernal-García,^{1,*} Simon White,¹ Hassan Jamal Latief,³ Alison Goldingay,³ Sven Rogge,³ Sergei Slussarenko,¹ Farzad Ghafari,^{1,†} Emanuele Polino,^{1,‡} and Nora Tischler^{1,§}

¹Queensland Quantum and Advanced Technologies Research Institute, Centre for Quantum Computation and Communication Technology,

Griffith University, Yuggera Country, Brisbane, Queensland, 4111 Australia

²Department of Physics, Humboldt University of Berlin, Berlin, 12489 Germany

³Centre for Quantum Computation and Communication Technology,

School of Physics, The University of New South Wales, Sydney, NSW 2052, Australia

(Dated: December 10, 2025)

Entangled states of photons form the foundation of quantum communication, computation, and metrology. Yet their generation remains fundamentally constrained: in the absence of intrinsic photon–photon interactions, the generation of such states is inherently probabilistic rather than deterministic. The prevalent technique of post-selection verifies the creation of an entangled state by detecting and thus destroying it. Heralding offers a solution in which measuring ancillary photons in auxiliary modes signals the state generation without the need to measure it. Here, we report an experiment to generate a three-mode two-photon NOON state, where the detection of a single photon in one heralding mode signifies the presence of the state in three target modes. We validate the generated state by estimating a fidelity of 0.823 ± 0.018 with respect to an ideal three-mode NOON state and certifying genuine multipartite entanglement. By virtue of the high success probability and small resource overhead of our scheme, our work provides a theoretical and experimental stepping stone for entangled multi-mode state generation, which is realizable with current technology. These multi-mode entangled states represent a key direction for linear optical quantum information that is complementary to multi-qubit state encoding.

Introduction— Entanglement is a defining feature of quantum mechanics, marking a clear departure from classical behaviour. Beyond their foundational significance, entangled states of photons also serve as a key resource for achieving quantum advantage in computing, communication, and metrology [1–3]. However, the generation of these photonic states remains generally a probabilistic process owing to negligible photon-photon interactions [4,5]. This leads to the fundamental challenge of determining when the desired state has been successfully generated. Most protocols for verifying state generation rely on post-selection, a destructive approach that measures all outputs to certify the produced state. Heralding overcomes this limitation by detecting ancillary photons in auxiliary modes, thereby providing an independent signal that flags the creation of the entangled state without disturbing it [6]. This capability is essential for fusion-based quantum computing [7], and for quantum communication, in which the heralding signal provides loss tolerance [8]. Heralding will likewise strengthen quantum metrology by optimizing the use of resources [9].

The heralded generation of maximally entangled states is an enduring research field that has recently been reigned. Notable experiments include the heralded generation of Bell states [10–15], two-mode NOON states [16–22] and most recently, the GHZ state [23–25]. Two-mode NOON states, $(|N,0\rangle + |0,N\rangle)/\sqrt{2}$, came to prominence as the gold standard for single-phase sensing in the absence of losses [26,27]. These states can be extended to multiple modes, where they again serve as a resource for important tasks in quantum metrology. For

example, multi-mode NOON states are useful for multiphase estimation [28–30] and distributed sensing [31], with potential applications ranging from quantum imaging and global clock synchronization to sensor networks and quantum algorithms [32–34].

Three-mode NOON states are maximally entangled states, defined as a coherent superposition of N photons in one mode and none in the other two modes: $|\psi_3^N\rangle = (|N,0,0\rangle + e^{i\alpha_1}|0,N,0\rangle + e^{i\alpha_2}|0,0,N\rangle)/\sqrt{3}$, where α_1 and α_2 are relative phases. Although proposals exist for generating three-mode NOON states spanning photons [35,36], atoms [37,38], and solitons [39], experimental realization remains extremely challenging: To date, a three-mode NOON state has only been reported in one experiment, and relied entirely on post-selection [29]. However, to allow for unrestricted usage, these states must be generated in a heralded fashion [9].

Here, we report the experimental generation of a three-mode NOON state,

$$|\psi_3^2\rangle = \frac{1}{\sqrt{3}} (|2,0,0\rangle + e^{i\alpha_1}|0,2,0\rangle + e^{i\alpha_2}|0,0,2\rangle), \quad (1)$$

whose successful creation is heralded by the detection of a single photon in an auxiliary mode. For this purpose, we theoretically introduce and experimentally demonstrate a scheme utilizing three single photons distributed across four modes. Our protocol employs an interferometric module, which acts jointly on the path and polarization degrees of freedom [1,41] and is optimized for simplicity and probability of success. The scheme features a nominal success probability of 0.25. We then

implement this protocol in a proof-of-principle photonic experiment and generate the heralded three-mode NOON state of Eq. (1). We achieve a success probability of 0.237 ± 0.009 and verify the state creation with a fidelity of $F = \langle \psi_3^2 | \rho | \psi_3^2 \rangle = 0.823 \pm 0.018$, where ρ denotes the experimentally prepared state. This verification relies on a tailored method that avoids challenges of full quantum state tomography. Moreover, the achieved fidelity surpasses the threshold for genuine multipartite entanglement by more than eight standard deviations.

Achieving high success probability and modest resource requirements, our work demonstrates a decisive advance towards practical schemes for heralded multi-mode entangled states generation, fundamental for linear optical quantum information.

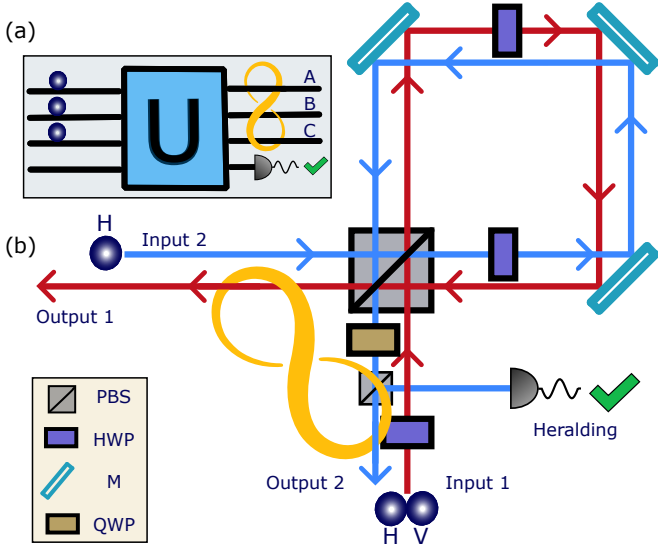


FIG. 1: Heralded generation of a three-mode NOON state via linear optics: (a) From an input of three single photons, a four-mode unitary transformation generates the desired coherent superposition of two photons in three modes (A,B,C) upon detecting a photon in the fourth mode. (b) The experimental setup for state generation consists of a displaced Sagnac interferometer constructed using a polarizing beam splitter and wave plates. The heralding process is schematically indicated, highlighting the projection onto the three-mode NOON state in the target modes upon detection of a photon in the heralding mode. The interferometer provides a stable and flexible platform for realizing four-mode unitary transformations [1,41]. QWP: quarter-wave plate; HWP: half-wave plate; M: mirror; PBS: polarizing beam splitter. The red and blue lines with arrows indicate the two spatial paths of the interferometer.

Unitary transformation for heralded state generation— We perform a four-mode unitary transformation on three single photons as illustrated by Fig. 1(a). We generate the desired two-photon three-mode state with a nominal

success probability $|\gamma|^2 = 0.25$, heralded by the detection of one photon in the auxiliary mode:

$$U |1, 1, 1, 0\rangle_{\text{input}} = \gamma |\psi_3^2\rangle_{\text{target}} |1\rangle_{\text{herald}} + \dots, \quad (2)$$

where the omitted terms correspond to the absence of the heralding signal and are therefore discarded. We use a combination of degrees of freedom to encode the four modes spanned by the two orthogonal polarizations and two path modes. We define the mode convention through the following single-photon states:

$$\begin{aligned} a_{\text{H, path1}}^\dagger |0\rangle &= |\text{100}\rangle_{\text{target}} |0\rangle_{\text{herald}}, \\ a_{\text{V, path1}}^\dagger |0\rangle &= |\text{010}\rangle_{\text{target}} |0\rangle_{\text{herald}}, \\ a_{\text{H, path2}}^\dagger |0\rangle &= |\text{001}\rangle_{\text{target}} |0\rangle_{\text{herald}}, \\ a_{\text{V, path2}}^\dagger |0\rangle &= |\text{000}\rangle_{\text{target}} |1\rangle_{\text{herald}}, \end{aligned} \quad (3)$$

where H and V denote horizontal and vertical polarizations, and the three modes of the target state are labeled A, B, and C in Fig. 1(a). Note that, if desired, the target state modes could be deterministically converted into purely path encoding.

We employ a gradient-descent search in the space of four-mode unitary transformations to identify unitaries that maximize the fidelity of the output state with respect to Eq. (1), given the separable input state $|1, 1, 1, 0\rangle$. Among the multiple solutions obtained with unit fidelity and success probability of 0.25, we select the unitary with the simplest experimental implementation based on the number of optical elements. The chosen transformation [see Sec. S1 of the Supplemental Material (SM)] is implemented by the setup shown in Fig. 1(b), a polarization-based displaced Sagnac interferometer.

Measurement protocol— Full quantum state tomography of the three-mode two-photon state is experimentally challenging, owing to the difficulty of characterizing coherent superpositions of multiphoton and vacuum components across several modes. Instead, we employ a targeted measurement protocol that exploits the structure of the three-mode NOON state in Eq. (1) to extract the state fidelity without complete tomographic reconstruction.

The measurement strategy relies on two types of measurements, all of which are conditioned on the heralding signal: a) projection onto the three-mode Fock states with two photons in total (i.e., populations); and b) probing information about coherences.

The coherence measurements rely on vacuum projection of individual modes k , reducing the heralded three-mode state ρ to the conditional states $\rho^{(ij)}$ within two-mode two-photon subspaces. Here $(i, j, k) \in \{A, B, C\}$ and are all distinct from each other. When mode k is projected onto vacuum, the remaining modes i and j are described by a conditional unnormalized density matrix

$\rho^{(ij)} = {}_k\langle 0|\rho|0\rangle_k$. For instance, when $k = C$, $\rho^{(AB)}$ exists in the subspace spanned by $\{|2,0\rangle_{AB}, |0,2\rangle_{AB}, |1,1\rangle_{AB}\}$ (see Fig. S2 of the SM). To extract the coherence between the $|2,0\rangle_{ij}$ and $|0,2\rangle_{ij}$ components, we perform a two-mode interferometric measurement consisting of a wave-plate transformation $U_{\text{meas}}(\theta) = \text{HWP}(\theta) \text{QWP}(\pi/4)$ followed by a polarizing beam splitter (PBS). Photon detectors at the PBS output ports record coincidence events, and the measured coincidence fringe C_{ij} as a function of the HWP angle θ is

$$C_{ij}(\theta) = \frac{A_{ij}}{2} + \frac{V_{ij}}{2} \cos(8\theta + \varphi_{ij}). \quad (4)$$

Here, the offset A_{ij} , visibility V_{ij} , and phase φ_{ij} are directly related to the elements of the prepared density matrix ρ (see S2.2 of the SM for the explicit derivation). In particular, the visibility V_{ij} quantifies the magnitude of coherence between the $|2,0\rangle_{ij}$ and $|0,2\rangle_{ij}$ basis states, while φ_{ij} represents its complex phase. Through the extraction of both V_{ij} and φ_{ij} from the sinusoidal fit, this measurement protocol enables complete reconstruction of the complex off-diagonal elements $\rho_{020,002}$, $\rho_{200,002}$, and $\rho_{200,020}$.

By repeating this procedure for all three mode combinations, projecting modes A , B , and C onto the vacuum in turn, we obtain three independent coincidence fringes $C_{BC}(\theta)$, $C_{AC}(\theta)$, and $C_{AB}(\theta)$. The coherence measurements alone allow for the evaluation of lower and upper bounds on the fidelity with respect to the three-mode NOON state of Eq. (1). Combined with the population measurements, the coherence measurements provide sufficient information to estimate the fidelity. Further details about the fidelity estimation are provided in Sec. S2 of the SM.

This measurement strategy enables robust state characterization without requiring full tomographic reconstruction.

Experimental implementation— The input state $|1,1,1,0\rangle$ is prepared by pumping a periodically poled potassium titanyl phosphate (ppKTP) crystal with a 775 nm pulsed picosecond laser. The crystal is pumped in two different locations to generate two pairs of orthogonally polarized photons via two simultaneous type-II spontaneous parametric down-conversion events. More details about the source are provided in the SM, see S3. Three of the four photons are sent into the state-generation setup (Fig. 1), while the fourth is used as a trigger. To overcome the non-deterministic preparation of the input state, $|1,1,1,0\rangle$, we certify the correct input state by considering four-fold coincidence events in the final measurements.

For both types of measurements, photon detection is performed using superconducting nanowire single-photon detectors (SNSPDs). Pseudo-photon number resolution is enabled by fanning out each target mode into two using a fiber beam splitter before detection [9]. To implement

the coherence measurements discussed above, we use a second displaced Sagnac interferometer, shown in the measurement panel of Fig. 2, followed by a polarization measurement. Coincidence probabilities as a function of θ are evaluated from coincidence counts. Thereafter, the required coherences are extracted from the data, and both an estimate of the fidelity and its lower and upper bounds with respect to Eq. (1) are determined.

Experimental results— Following the measurement protocol described above and further detailed in S2.2 of the SM, we evaluate the fidelity of the generated three-mode NOON state and find $F = 0.823 \pm 0.018$ with respect to Eq. (1), where $\alpha_1 = 1.568 \pm 0.030$ and $\alpha_2 = -0.262 \pm 0.033$ (in radians). This fidelity is compatible with the lower and upper bounds $F \in [0.817, 0.836]$, evaluated using only the coherence measurements shown in Fig. 3 (for more detail, see S2.3 of the SM). We estimate the experimental success probability of our scheme to be $|\gamma_{\text{exp}}|^2 = 0.237 \pm 0.009$. This is obtained by dividing the four-fold events in which heralding was successful using the unitary transformation, by the four-folds while implementing an identity transformation.

Furthermore, we study the presence of genuine multipartite entanglement (GME). Three-mode states exhibiting GME cannot be decomposed into a statistical mixture of states that are separable over any bipartition of the modes, i.e., they are not biseparable [42,43]. We certify GME by comparing the estimated fidelity with respect to Eq. (1), against the largest fidelity F_{bs} attainable with biseparable states.

Following the procedure described in the Appendix of Ref. [2], we determine F_{bs} by considering all bipartitions of the target state in Eq. (1). For each bipartition, we compute the Schmidt decomposition and identify the largest squared Schmidt coefficient. The maximum of these values across all bipartitions yields the GME threshold, $F_{\text{bs}} = 2/3$. The full derivation is provided in Sec. S2.4 of the SM. Our estimated fidelity exceeds this threshold by more than 8 standard deviations, unambiguously certifying genuine tripartite entanglement distributed across all three target modes.

Discussion— In this work, we demonstrate the heralded generation of a three-mode two-photon NOON state. To this end, we identify a suitable linear optical unitary for state generation providing unit fidelity, success probability of 0.25, and a resource-efficient implementation. Our scheme has a higher success probability than previous schemes [35,36], while reducing the number of input photons. We implement this scheme in a photonic experiment, where we rigorously characterize the state fidelity and certify genuine three-mode entanglement with high statistical significance.

In our experiment, the three photons incident on the circuit are generated probabilistically through two simultaneous SPDC processes, and their availability is ensured by four-fold coincidence detection at the output. This

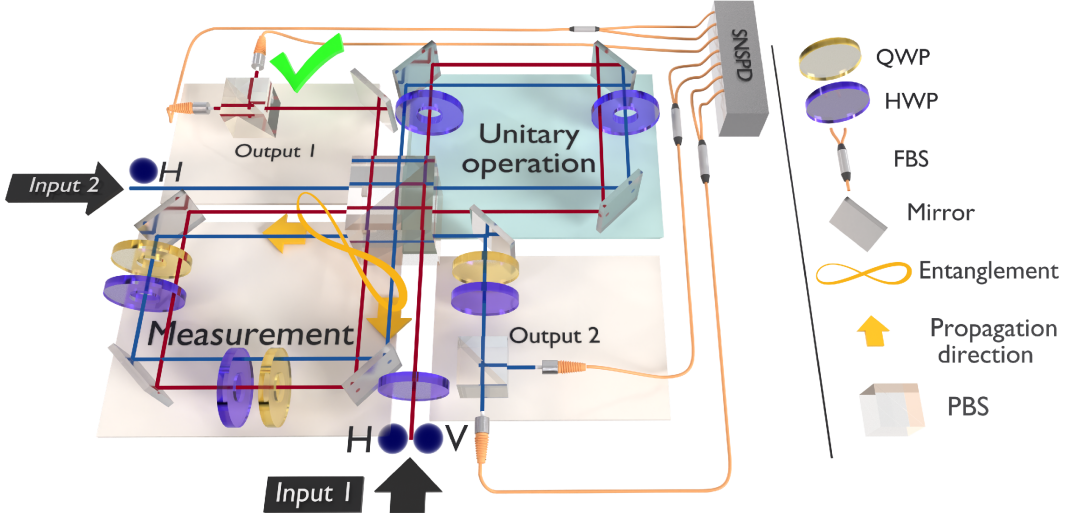


FIG. 2: **Interferometric scheme for heralded NOON state generation and characterization.** State preparation relies upon the HWP in input 1 and the first interferometer (unitary operation panel), followed by a QWP in the blue path in the subsequent interferometer. The measurement stage is realized using the second interferometer (measurement panel) and polarization projection in both outputs. The wave plates inside the interferometers have a hole in the center such that the polarization of only one path is transformed. Detection is performed using SNSPDs, with fiber beam splitters enabling pseudo-photon-number-resolving measurements on all three target modes. QWP: quarter-wave plate; HWP: half-wave plate; PBS: polarizing beam splitter; FBS: fiber beam splitter.

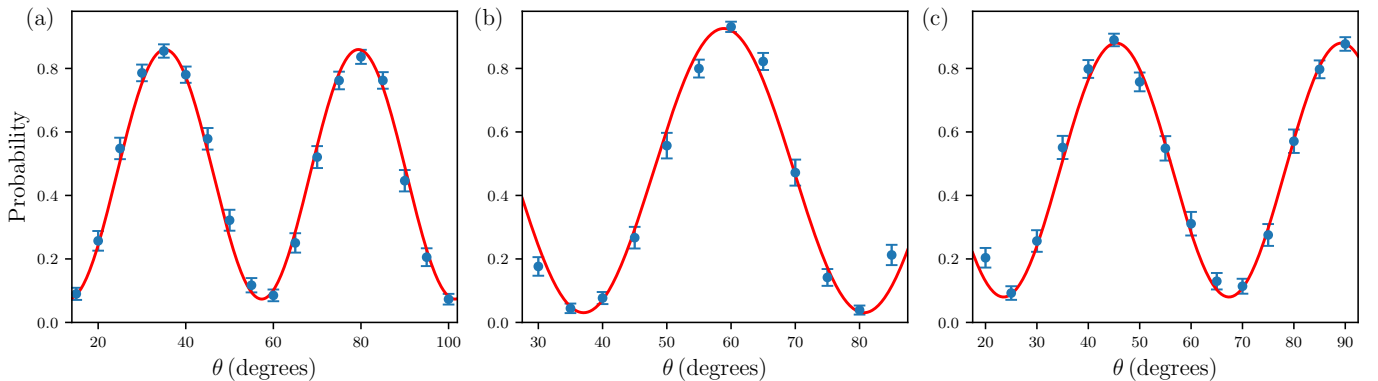


FIG. 3: The heralded three-mode state is projected onto a two-photon two-mode subspace by conditioning on vacuum in the remaining mode. To probe the coherence of the state in this subspace, we interfere the two modes after mapping them into the polarization basis of a single spatial mode. The resulting coincidence probabilities are shown as a function of the measurement half-wave plate angle θ for pairwise combinations of modes A and B (a), B and C (b), and A and C (c). Each probability data point (blue points) is obtained from an average of 1039 four-fold coincidence counts accumulated over 1800 s. The resulting data are fitted with the function given in Eq. (4) (red curve), and the uncertainties in the measured counts are estimated assuming Poissonian statistics.

choice of final photon counting is not a fundamental requirement: Using three SPDC sources, one could ensure the correct three-photon input state is available, where the detection of three single photons heralds their respective partners. The photon-number counting we employ also has the feature of mitigating the effect of losses, which are present in practical scenarios, independently of the choice of photon source. Importantly, this photon counting, based on the total number of photons across all

the modes, allows for full further processing of the state. By contrast, standard postselection, which occurs based on the number of photons in specific subsets of modes, imposes restrictions on subsequent interference of modes, severely limiting the use of post-selected states [9].

We have demonstrated a practical approach to generate a multi-mode NOON state from three single photons, using a bulk-optical setup that can be implemented in standard quantum optics laboratories. An interesting

future application of our heralded state would be multi-phase sensing [33].

Three-mode NOON states exhibit an almost unit theoretical fidelity ($|\langle \psi_{\text{opt}}^N | \psi_3^N \rangle|^2 \approx 0.9996$) with the state $|\psi_{\text{opt}}^N\rangle$ identified in Ref. [45], which is optimal for simultaneous multi-phase estimation. In our experiment, the experimentally generated state attains a fidelity of $\langle \psi_{\text{opt}}^2 | \rho | \psi_{\text{opt}}^2 \rangle = 0.836 \pm 0.019$ with respect to this optimal target state.

Overall, this work constitutes an important step toward the generation of increasingly complex heralded photonic states with more modes and photons [36,46–48]. This approach can be further extended through integrated photonics, providing a scalable and compact platform for implementing complex quantum circuits [49]. As a demonstration of heralded multi-mode entangled state generation, our work will contribute to future advances in quantum communication [31], multiphase sensing and quantum algorithms [34,45].

ACKNOWLEDGEMENTS

We acknowledge helpful discussions with Howard M. Wiseman. This work was supported by the Australian Research Council; N.T. is a recipient of an Australian Research Council Discovery Early Career Researcher Award (DE220101082); S.S. is a recipient of an Australian Research Council Future Fellowship (FT240100352); E.P. is a recipient of an Australian Research Council Discovery Early Career Researcher Award (DE250100762); the work was in part supported by ARC Grant No. CE170100012. S.P.S. acknowledges support from the Australian Government Research Training Program (RTP). F.G. is supported partly by the Griffith University Postdoctoral Fellowship (GUPF#58938). E.B. acknowledges support by BMFTR (project 13N16105). This material is based upon work supported by the Air Force Office of Scientific Research under Award No. FA2386-23-1-4086.

- [4] J. L. O’Brien, A. Furusawa, and J. Vučković, Photonic quantum technologies, *Nat. Photonics* **3**, 687 (2009).
- [5] A. Aspuru-Guzik and P. Walther, Photonic quantum simulators, *Nat. Phys.* **8**, 285 (2012).
- [6] S. Bartolucci, P. M. Birchall, M. Gimeno-Segovia, E. Johnston, K. Kieling, M. Pant, T. Rudolph, J. Smith, C. Sparrow, and M. D. Vidyashin, Creation of entangled photonic states using linear optics (2021), arXiv:2106.13825 [quant-ph].
- [7] S. Bartolucci *et al.*, Fusion-based quantum computation, *Nat. Commun.* **14**, 912 (2023).
- [8] C.-Y. Lu and J.-W. Pan, Quantum-dot single-photon sources for the quantum internet, *Nat. Nanotechnol.* **16**, 1294 (2021).
- [9] I. Forbes, F. Ghafari, E. Deacon, S. P. Singh, E. Lavie, P. Yard, R. Shaw, A. Laing, and N. Tischler, Heralded generation of entanglement with photons, *Rep. Prog. Phys.* **88**, 086002 (2025).
- [10] S. Barz, G. Cronenberg, A. Zeilinger, and P. Walther, Heralded generation of entangled photon pairs, *Nat. Photonics* **4**, 553 (2010).
- [11] T. Pittman, M. Donegan, M. Fitch, B. Jacobs, J. Franson, P. Kok, H. Lee, and J. Dowling, Heralded two-photon entanglement from probabilistic quantum logic operations on multiple parametric down-conversion sources, *IEEE Journal of Selected Topics in Quantum Electronics* **9**, 1478 (2003).
- [12] C. Śliwa and K. Banaszek, Conditional preparation of maximal polarization entanglement, *Phys. Rev. A* **67**, 030101 (2003).
- [13] C. Wagenknecht, C.-M. Li, A. Reingruber, X.-H. Bao, A. Goebel, Y.-A. Chen, Q. Zhang, K. Chen, and J.-W. Pan, Experimental demonstration of a heralded entanglement source, *Nat. Photonics* **4**, 549 (2010).
- [14] D. R. Hamel, L. K. Shalm, H. Hübel, A. J. Miller, F. Marsili, V. B. Verma, R. P. Mirin, S. W. Nam, K. J. Resch, and T. Jennewein, Direct generation of three-photon polarization entanglement, *Nat. Photonics* **8**, 801 (2014).
- [15] N. N. Skryabin *et al.*, Heralded generation of programmable two-qubit entangled states on a linear-optical platform, *Optica Quantum* **3**, 162 (2025).
- [16] H. S. Eisenberg, J. F. Hodelin, G. Khoury, and D. Bouwmeester, Multiphoton path entanglement by non-local bunching, *Phys. Rev. Lett.* **94**, 090502 (2005).
- [17] H. Kim, H. S. Park, and S.-K. Choi, Three-photon N00N states generated by photon subtraction from double photon pairs, *Opt. Express* **17**, 19720 (2009).
- [18] B. J. Smith, P. J. Mosley, J. S. Lundeen, and I. A. Walmsley, Heralded generation of two-photon NOON states for precision quantum metrology, in *Conference on Lasers and Electro-Optics/Quantum Electronics and Laser Science Conference and Photonic Applications Systems Technologies* (Optica Publishing Group, 2008) p. QFI5.
- [19] Y.-S. Ra, H.-T. Lim, J.-E. Oh, and Y.-H. Kim, Phase and amplitude controlled heralding of N00N states, *Opt. Express* **23**, 30807 (2015).
- [20] P. Vergyris, T. Meany, T. Lunghi, G. Sauder, J. Downes, M. J. Steel, M. J. Withford, O. Alibart, and S. Tanzilli, On-chip generation of heralded photon-number states, *Sci. Rep.* **6**, 35975 (2016).
- [21] J. C. F. Matthews, A. Politi, D. Bonneau, and J. L. O’Brien, Heralding two-photon and four-photon path entanglement on a chip, *Phys. Rev. Lett.* **107**, 163602 (2011).

* dn.bernalgarcia@gmail.com

† f.ghafari@griffith.edu.au

‡ e.polino@griffith.edu.au

§ n.tischler@griffith.edu.au

- [1] R. Prevedel, M. Aspelmeyer, C. Brukner, A. Zeilinger, and T. D. Jennewein, Photonic entanglement as a resource in quantum computation and quantum communication, *J. Opt. Soc. Am. B* **24**, 241 (2007).
- [2] J.-W. Pan, Z.-B. Chen, C.-Y. Lu, H. Weinfurter, A. Zeilinger, and M. Źukowski, Multiphoton entanglement and interferometry, *Rev. Mod. Phys.* **84**, 777 (2012).
- [3] F. Flamini, N. Spagnolo, and F. Sciarrino, Photonic quantum information processing: a review, *Rep. Prog. Phys.* **82**, 016001 (2018).

[22] M. W. Mitchell, J. S. Lundeen, and A. M. Steinberg, Super-resolving phase measurements with a multiphoton entangled state, *Nature* **429**, 161 (2004).

[23] S. Chen *et al.*, Heralded three-photon entanglement from a single-photon source on a photonic chip, *Phys. Rev. Lett.* **132**, 130603 (2024).

[24] H. Cao, L. M. Hansen, F. Giorgino, L. Carosini, P. Záhálka, F. Zilk, J. C. Loredo, and P. Walther, Photonic source of heralded Greenberger-Horne-Zeilinger states, *Phys. Rev. Lett.* **132**, 130604 (2024).

[25] N. Maring *et al.*, A versatile single-photon-based quantum computing platform, *Nat. Photonics* **18**, 603 (2024).

[26] J. P. Dowling, Quantum optical metrology – the lowdown on high-N00N states, *Cont. Phys.* **49**, 125 (2008).

[27] S. Slussarenko, M. M. Weston, H. M. Chrzanowski, L. K. Shalm, V. B. Verma, S. W. Nam, and G. J. Pryde, Unconditional violation of the shot-noise limit in photonic quantum metrology, *Nat. Photonics* **11**, 700 (2017).

[28] S. Hong, J. ur Rehman, Y.-S. Kim, Y.-W. Cho, S.-W. Lee, H. Jung, S. Moon, S.-W. Han, and H.-T. Lim, Quantum enhanced multiple-phase estimation with multi-mode N00N states, *Nat. Commun.* **12**, 5211 (2021).

[29] S. Hong, J. u. Rehman, Y.-S. Kim, Y.-W. Cho, S.-W. Lee, S.-Y. Lee, and H.-T. Lim, Practical sensitivity bound for multiple phase estimation with multi-mode N00N states, *Laser Photonics Rev.* **16**, 2100682 (2022).

[30] M. Namkung, D.-H. Kim, S. Hong, Y.-S. Kim, C. Lee, and H.-T. Lim, Optimal multiple-phase estimation with multi-mode NOON states against photon loss, *New J. Phys.* **26**, 073028 (2024).

[31] D.-H. Kim, S. Hong, Y.-S. Kim, K. Oh, S.-Y. Lee, C. Lee, and H.-T. Lim, Distributed quantum sensing with multi-mode N00N states, *Phys. Rev. Lett.* **135**, 050802 (2025).

[32] Z. Zhang and Q. Zhuang, Distributed quantum sensing, *Quantum Sci. Technol.* **6**, 043001 (2021).

[33] M. Barbieri, I. Gianani, A. Z. Goldberg, and L. L. Sánchez-Soto, Quantum multiphase estimation, *Contemp. Phys.* **65**, 112 (2024).

[34] V. Gebhart, A. Smerzi, and L. Pezzè, Bayesian quantum multiphase estimation algorithm, *Phys. Rev. Appl.* **16**, 014035 (2021).

[35] L. Zhang and K. W. C. Chan, Efficient methods for generating multi-mode noon states, *Opt. Commun.* **452**, 258 (2019).

[36] L. Zhang and K. W. C. Chan, Scalable generation of multi-mode NOON states for quantum multiple-phase estimation, *Sci. Rep.* **8**, 11440 (2018).

[37] S. Dengis, S. Wimberger, and P. Schlagheck, Multimode NOON-state generation with ultracold atoms via geodesic counterdiabatic driving, *Phys. Rev. A* **112**, 042610 (2025).

[38] G. Vanhaege, A. Bäcker, R. Ketzmerick, and P. Schlagheck, Creating triple-NOON states with ultracold atoms via chaos-assisted tunneling, *Phys. Rev. A* **106**, L011301 (2022).

[39] D. Tsarev, S. Osipov, R.-K. Lee, S. Kulik, and A. Alodjants, Quantum sensor network metrology with bright solitons, *Phys. Rev. A* **108**, 062612 (2023).

[1] B.-G. Englert, C. Kurtsiefer, and H. Weinfurter, Universal unitary gate for single-photon two-qubit states, *Phys. Rev. A* **63**, 032303 (2001).

[41] C.-J. Huang, H. Ma, Q. Yin, J.-F. Tang, D. Dong, C. Chen, G.-Y. Xiang, C.-F. Li, and G.-C. Guo, Realization of a quantum autoencoder for lossless compression of quantum data, *Phys. Rev. A* **102**, 032412 (2020).

[42] O. Gühne and G. Tóth, Entanglement detection, *Phys. Rep.* **474**, 1 (2009).

[43] C. Palazuelos and J. I. De Vicente, Genuine multipartite entanglement of quantum states in the multiple-copy scenario, *Quantum* **6**, 735 (2022).

[2] M. Bourennane, M. Eibl, C. Kurtsiefer, S. Gaertner, H. Weinfurter, O. Gühne, P. Hyllus, D. Bruß, M. Lewenstein, and A. Sanpera, Experimental Detection of multipartite entanglement using witness operators, *Phys. Rev. Lett.* **92**, 087902 (2004).

[45] P. C. Humphreys, M. Barbieri, A. Datta, and I. A. Walmsley, Quantum enhanced multiple phase estimation, *Phys. Rev. Lett.* **111**, 070403 (2013).

[46] S. Chin, J. Ryu, and Y.-S. Kim, Exponentially enhanced scheme for the heralded qudit Greenberger-Horne-Zeilinger state in linear optics, *Phys. Rev. Lett.* **133**, 253601 (2024).

[47] D. Bhatti and S. Barz, Heralding higher-dimensional Bell and Greenberger-Horne-Zeilinger states using multiport splitters, *New J. Phys.* **27**, 033006 (2025).

[48] G. Park, I. Matsumoto, T. Kiyohara, H. F. Hofmann, R. Okamoto, and S. Takeuchi, Realization of photon correlations beyond the linear optics limit, *Sci. Adv.* **9**, eadj8146 (2023).

[49] H. Wang, T. C. Ralph, J. J. Renema, C.-Y. Lu, and J.-W. Pan, Scalable photonic quantum technologies, *Nat. Mater.* **24**, 1883 (2025).

Supplemental Material for: Heralded generation of a three-mode NOON state

Sukhjit P. Singh,¹ Elnaz Bazzazi,² Diego N. Bernal-García,¹ Simon White,¹ Alison Goldingay,³ Hassan Jamal Latief,³ Sven Rogge,³ Sergei Slussarenko,¹ Farzad Ghafari,¹ Emanuele Polino,¹ and Nora Tischler¹

¹ *Queensland Quantum and Advanced Technologies Research Institute, Centre for Quantum Computation and Communication Technology, Griffith University, Yuggera Country, Brisbane, Queensland, 4111 Australia*

² *Department of Physics, Humboldt University of Berlin, Berlin, 12489 Germany*

³ *Centre for Quantum Computation and Communication Technology, School of Physics, The University of New South Wales, Sydney, NSW 2052, Australia*

(Dated: December 10, 2025)

S1. UNITARY TRANSFORMATION

The four-mode space relevant for our optical transformation is spanned by the hybrid path–polarization modes

$$\{|H, 1\rangle, |V, 1\rangle, |H, 2\rangle, |V, 2\rangle\},$$

where $|P, j\rangle$ denotes a single photon with polarization $P \in \{H, V\}$ in spatial path $j \in \{1, 2\}$. In this ordered basis,

$$|H, 1\rangle = \begin{pmatrix} 1 \\ 0 \\ 0 \\ 0 \end{pmatrix}, \quad |V, 1\rangle = \begin{pmatrix} 0 \\ 1 \\ 0 \\ 0 \end{pmatrix}, \quad |H, 2\rangle = \begin{pmatrix} 0 \\ 0 \\ 1 \\ 0 \end{pmatrix}, \quad |V, 2\rangle = \begin{pmatrix} 0 \\ 0 \\ 0 \\ 1 \end{pmatrix}. \quad (\text{S1})$$

For completeness, we recall the correspondence between these polarization–path modes and the occupation–number notation used in the main text. Acting on the vacuum $|0\rangle$,

$$\begin{aligned} a_{H,1}^\dagger |0\rangle &= |100\rangle_{\text{target}} |0\rangle_{\text{herald}} \equiv |H, 1\rangle, \\ a_{V,1}^\dagger |0\rangle &= |010\rangle_{\text{target}} |0\rangle_{\text{herald}} \equiv |V, 1\rangle, \\ a_{H,2}^\dagger |0\rangle &= |001\rangle_{\text{target}} |0\rangle_{\text{herald}} \equiv |H, 2\rangle, \\ a_{V,2}^\dagger |0\rangle &= |000\rangle_{\text{target}} |1\rangle_{\text{herald}} \equiv |V, 2\rangle. \end{aligned} \quad (\text{S2})$$

The four-mode unitary to generate a heralded three-mode NOON state from a separable input of three indistinguishable single photons, which is found through numerical optimization, can then be expressed in this basis as:

$$U = \begin{pmatrix} -\frac{1}{\sqrt{2}} & \frac{1}{\sqrt{6}} & -\frac{i}{\sqrt{6}} & \frac{1}{\sqrt{6}} \\ -\frac{1}{\sqrt{2}} & -\frac{1}{\sqrt{6}} & \frac{i}{\sqrt{6}} & -\frac{1}{\sqrt{6}} \\ 0 & -\sqrt{\frac{2}{3}} & -\frac{i}{\sqrt{6}} & \frac{1}{\sqrt{6}} \\ 0 & 0 & -\frac{1}{\sqrt{2}} & \frac{i}{\sqrt{2}} \end{pmatrix} \quad (\text{S3})$$

The experimental optical realization of this unitary transformation is illustrated in Fig. S1, where

$$U = U_{\text{QWP1}} U_{\text{PBS}} U_{\text{Mirror}} U_{\text{HWP3}} U_{\text{Mirror}} U_{\text{Mirror}} U_{\text{HWP2}} U_{\text{PBS}} U_{\text{HWP1}}.$$

Each wave plate implements a transformation that acts only on the spatial mode in which it is physically placed. Consequently, its action on the two-path, two-polarization Hilbert space is represented by a 4×4 block-diagonal unitary,

$$U_{\text{WP}} = \begin{pmatrix} V_{2 \times 2} & 0 \\ 0 & I_{2 \times 2} \end{pmatrix} \quad \text{or} \quad U_{\text{WP}} = \begin{pmatrix} I_{2 \times 2} & 0 \\ 0 & V_{2 \times 2} \end{pmatrix},$$

depending on whether the wave plate is located in the spatial path for input 1 or input 2, respectively. Here $V_{2 \times 2}$ is the polarization transformation applied to the affected path, while $I_{2 \times 2}$ denotes the identity acting on the unaffected path.

The single-path polarization transformations $V_{2 \times 2}$ corresponding to a half-wave plate (HWP) and a quarter-wave plate (QWP) oriented at an angle θ are (see Ref. [1]):

$$V_{\text{HWP}}(\theta) = -i \begin{pmatrix} \cos(2\theta) & \sin(2\theta) \\ \sin(2\theta) & -\cos(2\theta) \end{pmatrix},$$

$$V_{\text{QWP}}(\theta) = \frac{1}{\sqrt{2}} \begin{pmatrix} 1 - i \cos(2\theta) & -i \sin(2\theta) \\ -i \sin(2\theta) & 1 + i \cos(2\theta) \end{pmatrix}.$$

In the configuration used here, the wave plate angles are set as follows: $\text{HWP1} = \pi/8$, $\text{HWP2} = 0.848\pi$, $\text{HWP3} = 0$, and $\text{QWP1} = 3\pi/4$.

The polarizing beam splitter (PBS) separates horizontal and vertical polarizations into distinct spatial paths. In our convention, horizontally polarized photons are transmitted, while vertically polarized photons are routed to the opposite spatial mode and acquire a phase factor of i . In particular, a vertically polarized photon entering path 1 exits in path 2 with an additional phase i , and vice versa. Its action in the four-mode space is described by

$$U_{\text{PBS}} = \begin{pmatrix} 1 & 0 & 0 & 0 \\ 0 & 0 & 0 & i \\ 0 & 0 & 1 & 0 \\ 0 & i & 0 & 0 \end{pmatrix}.$$

A mirror imparts a relative phase ϕ between horizontal and vertical polarizations. In our setup, both mirrors affecting the two spatial modes introduce the same polarization-dependent phase on the vertical component. The corresponding unitary operation is expressed as

$$U_{\text{Mirror}} = \begin{pmatrix} 1 & 0 & 0 & 0 \\ 0 & e^{i\phi} & 0 & 0 \\ 0 & 0 & 1 & 0 \\ 0 & 0 & 0 & e^{i\phi} \end{pmatrix}.$$

The full setup shown in Fig. 2 of the main text was characterized using classical light. Laser light was injected into inputs 1 and 2 with four different polarizations: $|\text{Input}\rangle = |H\rangle, |V\rangle, |D\rangle$ and $|A\rangle$, and the output state was reconstructed by performing single-qubit polarization quantum state tomography in both of the spatial outputs. By fitting the experimental data with a theoretical model incorporating all the key setup parameters, such as wave plate angles and phase shifts, we reconstructed the experimentally realized unitary transformation. The retrieved parameters generate a unitary evolution which, for ideal input photons, would generate a state with a fidelity of 0.988 ± 0.004 with respect to the three-mode NOON state in Eq.(1) of the main text.

S2. MEASUREMENT PROTOCOL

S2.1. Fidelity estimation

We consider as target the three-mode, two-photon NOON state

$$|\psi_3^2\rangle = \frac{1}{\sqrt{3}} (|2, 0, 0\rangle + e^{i\alpha_1} |0, 2, 0\rangle + e^{i\alpha_2} |0, 0, 2\rangle), \quad (\text{S4})$$

where $\alpha_1, \alpha_2 \in [0, 2\pi)$ are real phase parameters. Given an experimentally prepared state ρ , the fidelity with respect to the target is

$$F = \langle \psi_3^2 | \rho | \psi_3^2 \rangle. \quad (\text{S5})$$

A straightforward expansion gives

$$F(\alpha_1, \alpha_2) = \frac{1}{3} \left[P_{200} + P_{020} + P_{002} + 2 \text{Re} \left(e^{-i\alpha_1} \rho_{200,020} + e^{-i\alpha_2} \rho_{200,002} + e^{-i(\alpha_2-\alpha_1)} \rho_{020,002} \right) \right], \quad (\text{S6})$$

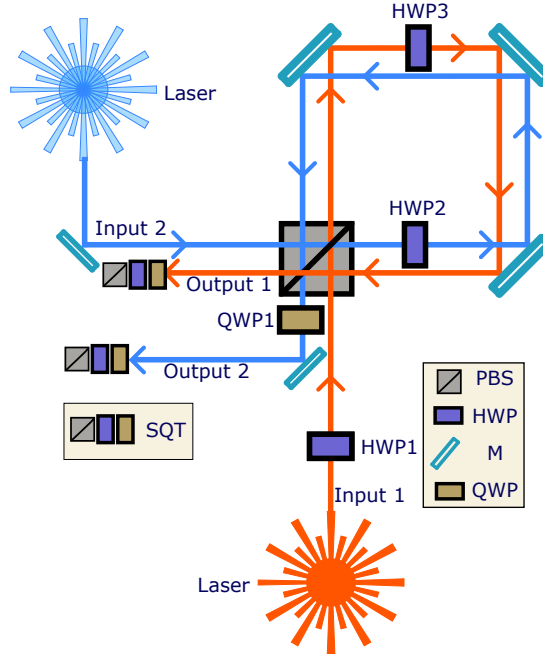


FIG. S1: Simplified schematic for the characterization of the setup with classical light. QWP: quarter-wave plate; HWP: half-wave plate; M: mirror; PBS: polarizing beam splitter; SQT: single-qubit tomography setup. The orange and blue lines with arrows indicate the two spatial paths of the interferometer.

where $P_{n_A n_B n_C} \equiv \rho_{n_A n_B n_C, n_A n_B n_C}$ denote the population terms.

Using $\text{Re}(e^{i\theta}z) = \text{Re}(z)\cos\theta - \text{Im}(z)\sin\theta$ for $z \in \mathbb{C}$, we obtain an explicit expression in terms of the real and imaginary parts of the coherence elements,

$$F(\alpha_1, \alpha_2) = \frac{1}{3} \left\{ P_{200} + P_{020} + P_{002} + 2[\text{Re}(\rho_{200,020}) \cos \alpha_1 + \text{Re}(\rho_{200,002}) \cos \alpha_2 + \text{Re}(\rho_{020,002}) \cos(\alpha_2 - \alpha_1)] + 2[\text{Im}(\rho_{200,020}) \sin \alpha_1 + \text{Im}(\rho_{200,002}) \sin \alpha_2 + \text{Im}(\rho_{020,002}) \sin(\alpha_2 - \alpha_1)] \right\}. \quad (\text{S7})$$

The three populations are experimentally accessible using the pseudo-photon-number-resolving detection method outlined in the main text. The off-diagonal elements $\rho_{200,020}$, $\rho_{200,002}$, and $\rho_{020,002}$ encode the pairwise two-mode coherences of the state and require dedicated interference measurements, which are discussed in the next subsection.

Since our target state is defined up to two relative phases α_1 and α_2 , we adopt an optimization strategy to find the best fit over all possible phase values. For a given set of experimentally measured density matrix elements, the estimated fidelity is then given by

$$F = \max_{\alpha_1, \alpha_2} F(\alpha_1, \alpha_2). \quad (\text{S8})$$

This optimization can be performed numerically using standard gradient-based or global optimization algorithms. The optimal phases $(\alpha_1^{\text{opt}}, \alpha_2^{\text{opt}})$ obtained from the best fidelity fit provide information about the relative phases present in the experimentally prepared state, and return the fidelity between the experimentally prepared state ρ and the closest multi-mode NOON state.

S2.2. Measurement strategy for coherence extraction

The experimental characterization of the three-mode state ρ relies on a sequence of projective measurements designed to extract the two-mode coherence terms of the density matrix. Fig. S2 provides a schematic overview of the protocol, which proceeds as follows:

1. **Vacuum projection:** One of the three modes is projected onto the vacuum state $|0\rangle$, effectively reducing the system to a two-mode subspace.

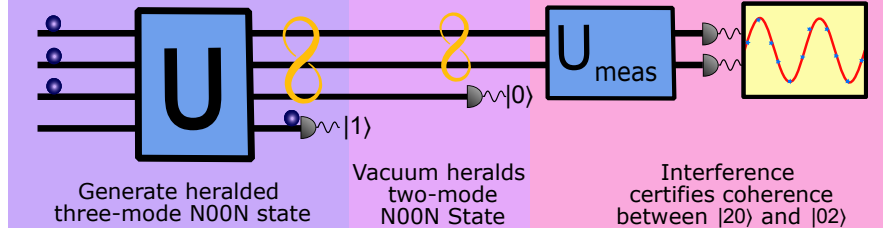


FIG. S2: Schematic summary of the measurement sequence used to extract the interference fringes presented in Fig 3 of the main text.

2. **Unitary transformation:** The remaining two modes undergo a parameterized unitary transformation $U_{\text{meas}}(\theta)$, implemented by a sequence of wave plates, before entering a polarizing beam splitter (PBS).
3. **Coincidence detection:** The probability of the simultaneous detection of one photon in each output port of the PBS is recorded as a function of the rotation angle θ .

This procedure is repeated three times, projecting each of the three modes onto vacuum in turn, and yielding three coincidence curves, $C_{BC}(\theta)$, $C_{AC}(\theta)$, and $C_{AB}(\theta)$, corresponding to vacuum projection of modes A , B , and C , respectively.

Consider now projecting mode $k \in \{A, B, C\}$ onto the vacuum state. The (unnormalized) state of the remaining modes is

$$\rho^{(ij)} = \langle 0|_k \rho |0\rangle_k, \quad (\text{S9})$$

with $\{i, j, k\}$ a permutation of $\{A, B, C\}$. The corresponding normalized state is

$$\rho'^{(ij)} = \frac{\rho^{(ij)}}{\rho_{20,20}^{(ij)} + \rho_{02,02}^{(ij)} + \rho_{11,11}^{(ij)}}, \quad (\text{S10})$$

Explicitly, for each choice of projected mode, we define:

$$\text{Mode } A \text{ projected: } \rho_{n_B n_C, m_B m_C}^{(BC)} = \rho_{0 n_B n_C, 0 m_B m_C}, \quad (\text{S11a})$$

$$\text{Mode } B \text{ projected: } \rho_{n_A n_C, m_A m_C}^{(AC)} = \rho_{n_A 0 n_C, m_A 0 m_C}, \quad (\text{S11b})$$

$$\text{Mode } C \text{ projected: } \rho_{n_A n_B, m_A m_B}^{(AB)} = \rho_{n_A n_B 0, m_A m_B 0}. \quad (\text{S11c})$$

The unitary transformation $U(\theta)$ acting on modes i and j is implemented through the wave plate sequence

$$U(\theta) = \text{HWP}(\theta) \text{QWP}(\pi/4), \quad (\text{S12})$$

where $\text{QWP}(\phi)$ and $\text{HWP}(\phi)$ denote quarter-wave and half-wave plates, respectively, with fast axes oriented at angle ϕ relative to a laboratory-fixed reference frame. This configuration mixes the real and imaginary parts of the coherence term $\rho_{20,02}^{(ij)}$, enabling their simultaneous extraction from the measured fringe. After the combined unitary transformation and PBS operation, the density matrix in the measurement basis is

$$\tilde{\rho}^{(ij)}(\theta) = U_{\text{PBS}} U(\theta) \rho'^{(ij)} U(\theta)^\dagger U_{\text{PBS}}^\dagger, \quad (\text{S13})$$

and the coincidence probability of detecting one photon in each output port is

$$C_{ij}(\theta) = \langle 1, 1 | \tilde{\rho}^{(ij)}(\theta) | 1, 1 \rangle. \quad (\text{S14})$$

For the wave plate configuration in Eq. (S12), $C_{ij}(\theta)$ has the sinusoidal form

$$C_{ij}(\theta) = \frac{A_{ij}}{2} + \frac{V_{ij}}{2} \cos(8\theta + \varphi_{ij}), \quad (\text{S15})$$

where A_{ij} is the offset, V_{ij} the visibility, and φ_{ij} the fringe phase. These parameters are related to density matrix elements via

$$A_{ij} = \frac{\rho_{20,20}^{(ij)} + \rho_{02,02}^{(ij)}}{\rho_{20,20}^{(ij)} + \rho_{02,02}^{(ij)} + \rho_{11,11}^{(ij)}}, \quad (\text{S16a})$$

$$V_{ij} = \frac{2|\rho_{20,02}^{(ij)}|}{\rho_{20,20}^{(ij)} + \rho_{02,02}^{(ij)} + \rho_{11,11}^{(ij)}}, \quad (\text{S16b})$$

$$\varphi_{ij} = \arg(\rho_{20,02}^{(ij)}); \quad (\text{S16c})$$

with $\rho_{20,02}^{(ij)} = |\rho_{20,02}^{(ij)}| e^{-i\varphi_{ij}}$. The visibility V_{ij} then encodes the magnitude of the two-photon coherence, while the phase φ_{ij} relates to its complex argument. Since $\rho'^{(ij)}$ is normalized, $\rho'_{20,20}^{(ij)} + \rho'_{02,02}^{(ij)} + \rho'_{11,11}^{(ij)} = 1$, we may equivalently write $A_{ij} = 1 - \rho'_{11,11}^{(ij)}$, showing that the offset A_{ij} reflects the population of the $|1,1\rangle$ component.

Thus, by fitting the measured coincidence curves $C_{ij}(\theta)$ to Eq. (S15), we can extract both the magnitude and phase of the coherence element $\rho_{20,02}^{(ij)}$ for each bipartition, providing the information required for the fidelity analysis in the main text.

S2.3. Fidelity bounds from coherence measurements without populations

The measurement protocol described in the previous subsection provides direct access to the two-mode coherence elements of the three-mode state ρ . Although our experiment additionally provides pseudo-photon-number-resolved population measurements, it is instructive to also consider a more conservative scenario in which population information is unavailable or unreliable. We show here that the coincidence measurements alone already determine *rigorous upper and lower bounds* on the fidelity with respect to the target three-mode NOON state in Eq. (S4).

The key observation is that the definitions in Eqs. (S16a) and (S16b) when combined with the positivity constraint

$$|\rho_{ij}|^2 \leq \rho_{ii}\rho_{jj}, \quad (\text{S17})$$

valid for any density matrix, impose nontrivial restrictions on the possible population distributions consistent with the observed data. To formalize this approach, we introduce a convenient notation for the relevant three-mode populations,

$$P_A = \rho_{200,200}, \quad P_B = \rho_{020,020}, \quad P_C = \rho_{002,002}, \quad (\text{S18a})$$

$$P_{AB} = \rho_{110,110}, \quad P_{AC} = \rho_{101,101}, \quad P_{BC} = \rho_{011,011}; \quad (\text{S18b})$$

and define dimensionless population ratios,

$$r_B = \frac{P_B}{P_A}, \quad r_C = \frac{P_C}{P_A}, \quad r_{AB} = \frac{P_{AB}}{P_A}, \quad r_{AC} = \frac{P_{AC}}{P_A}, \quad r_{BC} = \frac{P_{BC}}{P_A}. \quad (\text{S19})$$

Using these ratios, the offsets and visibilities obtained from the three coincidence curves may be written as

$$A_{BC} = \frac{r_B + r_C}{r_B + r_C + r_{BC}}, \quad V_{BC} = \frac{2|\rho_{020,002}|}{P_B + P_C + P_{BC}}, \quad (\text{S20a})$$

$$A_{AB} = \frac{1 + r_B}{1 + r_B + r_{AB}}, \quad V_{AB} = \frac{2|\rho_{200,020}|}{P_A + P_B + P_{AB}}, \quad (\text{S20b})$$

$$A_{AC} = \frac{1 + r_C}{1 + r_C + r_{AC}}, \quad V_{AC} = \frac{2|\rho_{200,002}|}{P_A + P_C + P_{AC}}. \quad (\text{S20c})$$

Applying the inequality in Eq. (S17) to each relevant coherence term yields three constraints on the population ratios,

$$\frac{V_{AB}^2}{A_{AB}^2} (1 + r_B)^2 \leq 4r_B, \quad (\text{S21a})$$

$$\frac{V_{AC}^2}{A_{AC}^2} (1 + r_C)^2 \leq 4r_C, \quad (\text{S21b})$$

$$\frac{V_{BC}^2}{A_{BC}^2} (r_B + r_C)^2 \leq 4r_B r_C. \quad (\text{S21c})$$

These inequalities define the feasible region \mathcal{R} in (r_B, r_C) space compatible with the observed visibilities and offsets, independently of any direct population measurement.

Furthermore, the fidelity in Eq. (S7) can be expressed as

$$F(\alpha_1, \alpha_2) = \frac{P_A}{3} \left[1 + r_B + r_C + \frac{V_{AB}}{A_{AB}} (1 + r_B) \cos(\alpha_1 - \varphi_{AB}) + \frac{V_{AC}}{A_{AC}} (1 + r_C) \cos(\alpha_2 - \varphi_{AC}) + \frac{V_{BC}}{A_{BC}} (r_B + r_C) \cos(\alpha_2 - \alpha_1 - \varphi_{BC}) \right], \quad (\text{S22})$$

where α_1 and α_2 are the two relative phases of the state in Eq. (S4), and P_A can be written as

$$P_A = \left[1 + (1 + r_B) \left(\frac{1}{A_{AB}} - 1 \right) + (1 + r_C) \left(\frac{1}{A_{AC}} - 1 \right) + \frac{r_B + r_C}{A_{BC}} \right]^{-1}. \quad (\text{S23})$$

As above, the phases must be fitted to obtain the maximum achievable fidelity consistent with the data. To simplify this optimization, we combine the first two cosine terms using standard trigonometric identities. Defining

$$S_A = \frac{V_{AB}}{A_{AB}} (1 + r_B), \quad S_C = \frac{V_{AC}}{A_{AC}} (1 + r_C), \quad (\text{S24})$$

and letting

$$\Delta = \alpha_2 - \alpha_1 + \varphi_{AB} - \varphi_{AC}, \quad (\text{S25})$$

we obtain

$$S_A \cos(\alpha_1 - \varphi_{AB}) + S_C \cos(\alpha_2 - \varphi_{AC}) = R \cos(\alpha_1 - \varphi_{AB} + \phi), \quad (\text{S26})$$

where

$$R = \sqrt{S_A^2 + S_C^2 + 2S_A S_C \cos \Delta}, \quad \phi = \arctan \left[\frac{S_C \sin \Delta}{S_A + S_C \cos \Delta} \right]. \quad (\text{S27})$$

Maximizing F over α_1 is now straightforward by choosing $\alpha_1 = \varphi_{AB} - \phi$, which yields

$$\bar{F}(\delta) = \frac{P_A}{3} \left[1 + r_B + r_C + R + \frac{V_{BC}}{A_{BC}} (r_B + r_C) \cos(\delta - \varphi_{BC}) \right], \quad (\text{S28})$$

where $\delta = \alpha_2 - \alpha_1$ is the remaining free phase, and P_A is given by Eq. (S23). For fixed (r_B, r_C) , the maximum fidelity is obtained by optimizing $\bar{F}(\delta)$ over δ .

The full optimization used to compute fidelity bounds is therefore:

1. Extract V_{ij} , φ_{ij} and A_{ij} from the measured coincidence fringes.
2. Determine the feasible region \mathcal{R} in (r_B, r_C) satisfying the constraints in Eqs. (S21).
3. For each $(r_B, r_C) \in \mathcal{R}$, compute

$$F_{\max}(r_B, r_C) = \max_{\delta} \bar{F}(\delta).$$

4. The fidelity bounds follow as

$$F_{\text{lower}} = \min_{(r_B, r_C) \in \mathcal{R}} F_{\max}(r_B, r_C), \quad F_{\text{upper}} = \max_{(r_B, r_C) \in \mathcal{R}} F_{\max}(r_B, r_C). \quad (\text{S29})$$

This procedure provides rigorous fidelity bounds $F \in [F_{\text{lower}}, F_{\text{upper}}]$ using *only* the information contained in the coincidence measurements. When population measurements are available, the population ratios (r_B, r_C) are fixed uniquely, collapsing the bounds to a single fidelity value.

Applying this method to the measured fringes shown in Fig. 3 of the main text yields $F \in [0.818, 0.836]$, with experimental uncertainties propagated throughout the optimization.

S2.4. Genuine tripartite entanglement threshold for the three-mode two-photon NOON state

To certify genuine tripartite entanglement, we determine the maximal fidelity between a target pure tripartite state $|\psi\rangle$ and any biseparable state. To obtain this general bound, we follow the procedure described in the Appendix of Ref. [2]. For completeness, and to keep this work self-contained, we reproduce the argument here.

A mixed state σ on parties A, B, C is biseparable if it can be written as a convex combination of pure states that are separable with respect to at least one bipartition ($A|BC$, $B|AC$, or $C|AB$) [2]. However, since any mixed state is a convex combination of pure states and the fidelity $F(|\psi\rangle, \sigma) = \langle\psi|\sigma|\psi\rangle$ is linear, the maximum fidelity with respect to biseparable states is always achieved by a pure biseparable state. We therefore define the biseparable fidelity bound as

$$F_{\text{bs}} := \max_{|\phi\rangle \in \mathcal{B}} |\langle\phi|\psi\rangle|^2, \quad (\text{S30})$$

where \mathcal{B} denotes the set of pure biseparable states. Thus, any state ρ satisfying $F(|\psi\rangle, \rho) > F_{\text{bs}}$ is certified to be genuinely tripartite entangled.

To determine F_{bs} , we first fix a bipartition, say $A|BC$, and choose orthonormal bases $\{|i\rangle_A\}$ and $\{|j\rangle_{BC}\}$ for the corresponding subsystems. In this basis, any normalized pure tripartite state $|\psi\rangle$ can be written as

$$|\psi\rangle = \sum_{i,j} C_{ij} |i\rangle_A |j\rangle_{BC}, \quad (\text{S31})$$

for some complex coefficient matrix C . Any pure product state across the same bipartition has the form

$$|\phi\rangle = |a\rangle|b\rangle = \sum_{i,j} a_i b_j |i\rangle_A |j\rangle_{BC}, \quad (\text{S32})$$

where the vectors $\mathbf{a} = (a_1, a_2, \dots)^T$ and $\mathbf{b} = (b_1, b_2, \dots)^T$ are normalized, $\sum_i |a_i|^2 = \sum_j |b_j|^2 = 1$. The overlap between the product state $|\phi\rangle$ and the target state $|\psi\rangle$ is then

$$\langle\phi|\psi\rangle = \sum_{i,j} a_i^* C_{ij} b_j^* = \mathbf{a}^\dagger C \mathbf{b}^*. \quad (\text{S33})$$

Maximizing the fidelity $|\langle\phi|\psi\rangle|^2$ over product states $|\phi\rangle$ is therefore equivalent to maximizing $|\mathbf{a}^\dagger C \mathbf{b}^*|^2$ over all normalized vectors \mathbf{a} and \mathbf{b} .

To obtain a useful upper bound, we perform a singular value decomposition $C = U\Sigma V^\dagger$, where U and V are unitary and $\Sigma = \text{diag}(\sigma_1, \sigma_2, \dots)$ collects the singular values $\sigma_k \geq 0$ of C . Introducing the normalized vectors $\mathbf{x} = U^\dagger \mathbf{a}$ and $\mathbf{y} = V^\dagger \mathbf{b}^*$, we obtain

$$|\mathbf{a}^\dagger C \mathbf{b}^*|^2 = |\mathbf{a}^\dagger U\Sigma V^\dagger \mathbf{b}^*|^2 = |\mathbf{x}^\dagger \Sigma \mathbf{y}|^2 \quad (\text{S34})$$

$$= \left| \sum_k \sigma_k x_k^* y_k \right|^2 \leq \sigma_{\max}^2 \left| \sum_k x_k^* y_k \right|^2, \quad (\text{S35})$$

where $\sigma_{\max} = \max_k \sigma_k$ is the largest singular value of C . Further, by the Cauchy–Schwarz inequality,

$$\left| \sum_k x_k^* y_k \right|^2 \leq \sum_k |x_k|^2 \sum_k |y_k|^2 = 1, \quad (\text{S36})$$

and the fidelity then satisfies

$$|\langle\phi|\psi\rangle|^2 = |\mathbf{a}^\dagger C \mathbf{b}^*|^2 \leq \sigma_{\max}^2. \quad (\text{S37})$$

Therefore, for the bipartition $A|BC$,

$$\max_{|\phi\rangle \in A|BC} |\langle\phi|\psi\rangle|^2 = \max_k \sigma_k^2. \quad (\text{S38})$$

The same optimization can be carried out for the remaining bipartitions $B|AC$ and $C|AB$. We therefore obtain the biseparable fidelity bound as

$$F_{\text{bs}} = \max \left\{ \max_k \sigma_k^2(A|BC), \max_k \sigma_k^2(B|AC), \max_k \sigma_k^2(C|AB) \right\}, \quad (\text{S39})$$

that is, the maximum singular value squared across all three possible bipartitions of the system. Finally, we recall that the singular values of the coefficient matrix C appearing in Eq. (S31) are precisely the Schmidt coefficients of $|\psi\rangle$ with respect to the chosen bipartition. Then, F_{bs} is simply the largest squared Schmidt coefficient of $|\psi\rangle$ when considering all bipartitions of the tripartite Hilbert space. A fidelity exceeding this value therefore certifies genuine tripartite entanglement.

We now apply this general result to the three-mode two-photon NOON state $|\psi_3^2\rangle$ in Eq. (S4), which is symmetric under permutations of the modes. For the partition $A|BC$ we introduce the orthonormal states

$$|\varphi_1\rangle = \frac{1}{\sqrt{2}} (e^{i\alpha_1} |20\rangle + e^{i\alpha_2} |02\rangle), \quad |\varphi_2\rangle = |00\rangle, \quad (\text{S40})$$

so that

$$|\psi_3^2\rangle = \sqrt{\frac{2}{3}} |0\rangle |\varphi_1\rangle + \sqrt{\frac{1}{3}} |2\rangle |\varphi_2\rangle. \quad (\text{S41})$$

Then, the coefficient matrix C will be given by

$$C = \begin{pmatrix} \sqrt{\frac{2}{3}} & 0 \\ 0 & \sqrt{\frac{1}{3}} \end{pmatrix}, \quad (\text{S42})$$

and the Schmidt coefficients for $A|BC$ are therefore $\sqrt{2/3}$ and $\sqrt{1/3}$. By symmetry, the same Schmidt spectrum holds for the bipartitions $B|AC$ and $C|AB$. Thus, the largest squared Schmidt coefficient over all bipartitions is

$$F_{\text{bs}} = \frac{2}{3}, \quad (\text{S43})$$

independent of the phases α_1 and α_2 . Any state ρ with $F(|\phi\rangle, \rho) > 2/3$ is therefore genuinely tripartite entangled.

S3. EXPERIMENTAL DETAILS

S3.1. Input state source

The input state $|1, 1, 1, 0\rangle$ is generated using a multiphoton source based on the design of Ref. [3,4], which produces four single photons in four modes from two simultaneous type-II spontaneous parametric down-conversion (SPDC) events within a beam-displacer interferometer. A horizontally polarized picosecond 775 nm pump beam first passes through a half-wave plate (HWP) that transforms its polarization to an equal superposition of H and V components, which are then spatially separated into two horizontally displaced beams by the first beam displacer (BD). Two subsequent HWPs rotate both beams to horizontal polarization, suitable for type-II down-conversion, while matching their optical paths. These beams pump a 15-mm-long periodically poled potassium titanyl phosphate (ppKTP) crystal in two distinct locations, allowing for degenerate type-II SPDC. A second BD vertically separates the signal and idler photons, producing four down-converted photons in four distinct beams. Three additional HWPs then rotate the polarizations so that single photons in the two left beams are H-polarized and the two right beams are V-polarized. This configuration allows the signal photons from the two down-conversion regions to be recombined into one path by the third BD, and likewise for the idler photons. At the output of the BD interferometer, two vertically separated beams remain, each containing a pair of orthogonally polarized photons. The generated state can be written as $|1_H, 1_V\rangle_{\text{top}} |1_H, 1_V\rangle_{\text{bottom}}$. A D-shaped mirror separates the propagation paths of the top and bottom beams, which are subsequently collimated, spectrally filtered with a 1-nm band-pass filter centered at 1550 nm, and coupled into single-mode fibers. The V-polarized photon in the bottom beam is detected with an SNSPD, while the remaining H-polarized photon, is sent to input 2 of the state generation setup. The bottom-beam pair, $|1_H, 1_V\rangle_{\text{bottom}}$, is sent to input 1. This procedure yields the separable input state used in our experiment: $|1_H, 0_V\rangle_{\text{Input2}} |1_H, 1_V\rangle_{\text{Input1}}$.

S3.2. Measurements of interference fringes and populations

The interference fringes (Fig. 3 of the main text) were measured using the pseudo-photon-number-resolution detection mentioned in the main text. The four-fold coincidence probabilities were normalized by taking into account the

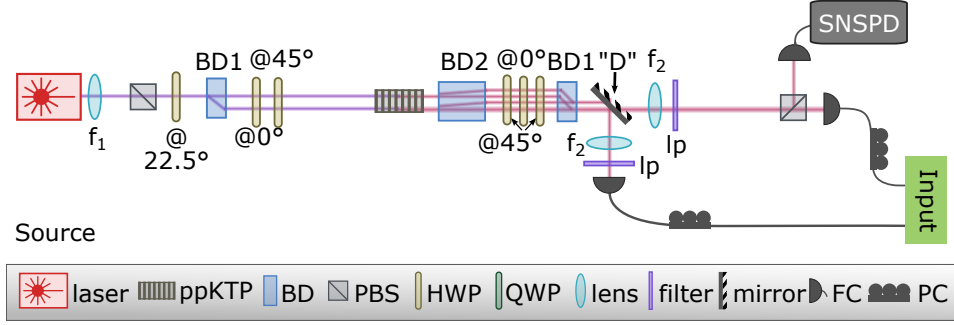


FIG. S3: **Input state generation.** Schematic of the source, as detailed in Sec. . Abbreviations: ppKTP – periodically poled potassium titanyl phosphate; BD – (polarizing) beam displacer; PBS – polarizing beam splitter; HWP – half-wave plate; QWP – quarter-wave plate; FC – (single-mode) fiber coupler; BS – (fiber) beam splitter; PC – (fiber) polarization controller; SNSPD – superconducting nanowire single-photon detector; lp – long-pass filter; bp – band-pass filter; “D” – D-shaped mirror with a horizontal cut (not visible in top view). BD2 provides a vertical beam displacement, illustrated in the schematic by the slight vertical separation of beam pairs (source design based on [4]).

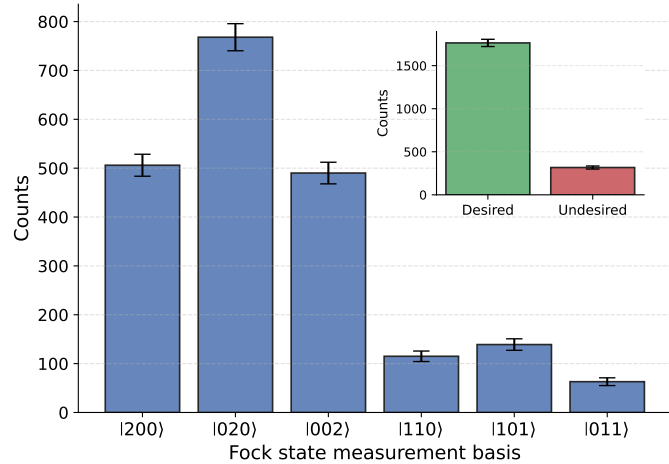


FIG. S4: **Populations:** Photon-number populations measured in the Fock basis. Dominant contributions arise from the NOON components: $|200\rangle$, $|020\rangle$ and $|002\rangle$. Their sum and the sum of the undesired events ($|110\rangle$, $|101\rangle$, and $|011\rangle$) are shown for comparison in the inset.

$|1,1\rangle$, $|2,0\rangle$ and $|0,2\rangle$ terms:

$$P_{|1,1\rangle} = \frac{\text{Counts}_{|1,1\rangle}}{\text{Counts}_{|1,1\rangle} + \text{Counts}_{|2,0\rangle} + \text{Counts}_{|0,2\rangle}}. \quad (\text{S44})$$

The experimentally observed visibilities for the three sets of probability curves are $81.9 \pm 3.6\%$ for modes (A,B), $92.0 \pm 2.8\%$ for modes (B,C) and $81.2 \pm 4.0\%$ for modes (A,C) of the state $|\psi_3^2\rangle$. The centers of oscillation for the three curves in Fig. 3 of the main text, obtained by fitting the data with Eq. (S15), are 0.467 ± 0.005 (C_{AB}), 0.478 ± 0.007 (C_{BC}), and 0.480 ± 0.006 (C_{AC}). These values are close to the ideal of 0.5 and the slight reduction is due to the presence of undesired terms in the generated state. The sum of the measured populations is 0.847 ± 0.038 and the recorded counts are shown in Fig. S4.

* dn.bernalgarcia@gmail.com

† f.ghafari@griffith.edu.au

‡ e.polino@griffith.edu.au

§ n.tischler@griffith.edu.au

- [1] B.-G. Englert, C. Kurtsiefer, and H. Weinfurter, Universal unitary gate for single-photon two-qubit states, *Phys. Rev. A* **63**, 032303 (2001).
- [2] M. Bourennane, M. Eibl, C. Kurtsiefer, S. Gaertner, H. Weinfurter, O. Gühne, P. Hyllus, D. Bruß, M. Lewenstein, and A. Sanpera, Experimental Detection of multipartite entanglement using witness operators, *Phys. Rev. Lett.* **92**, 087902 (2004).
- [3] L. K. Shalm *et al.*, Strong loophole-free test of local realism, *Phys. Rev. Lett.* **115**, 250402 (2015).
- [4] N. Tischler, F. Ghafari, T. J. Baker, S. Slussarenko, R. B. Patel, M. M. Weston, S. Wollmann, L. K. Shalm, V. B. Verma, S. W. Nam, H. C. Nguyen, H. M. Wiseman, and G. J. Pryde, Conclusive experimental demonstration of one-way Einstein-Podolsky-Rosen Steering, *Phys. Rev. Lett.* **121**, 100401 (2018).